NASA TM- 77722

NASA TECHNICAL MEMORANDUM

NASA TM-77722

A NEW METHOD OF EVALUATING THE SIDE WALL INTERFERENCE EFFECT ON AIRFOIL ANGLE OF ATTACK BY SUCTION FROM THE SIDE WALLS

Hideo Sawada, Seizo Sakakibara, Mamoru Sato, Hiroshi Kanda, Toshio Karasawa

Translation of "Sokuhtkikarano suikomi ni yogu tsubasa gata geikakueno sokuhekikansho kohkano atarashi". National Aerospace Laboratory, Tokyo, Japan, Report NAL-TR-680, August 1981, pp 1 - 18.

NATIONAL AERONAUTICS AND SPACE ADMINISTRATION
WASHINGTON D.C. 20546 AUGUST 1984

STANDARD TITLE PAGE

1. Report No. NASA TM-77722	2. Government Accession No.	3. Recipient's Catalog No.
4. Title and Subtitle A NEW METHOD OF EVALUATING THE SIDE WALL INTERFERENCE EFFECT ON AIRFOIL ANGLE OF ATTACK BY SUCTION FROM THE SIDE WALLS		5. Report Date AUGUST 1984 6. Performing Organization Code
7. Author(s) Hideo Sawada, Seizo Sakakibara, Mamoru Sato, Hiroshi Kanda Toshio Karasawa		8. Performing Organization Report No. 10. Work Unit No.
9. Performing Organization Name and Address SCITRAN Box 5456 Santa Barbara, CA 93108		11. Contract or Grant No. NASw- 3542 13. Type of Report and Period Covered Translation
12. Sponsoring Agency Name and Address National Aeronautics and Space Administration Washington, D.C. 20546		14. Sponsoring Agency Code

15. Supplementary Notes

Translation of "Sokuhtkikarano suikomi ni yogu tsubasa gata geikakueno sokuhekikansho kohkano atarashi". National Aerospace Laboratory, Tokyo, Japan, Report NAL-TR-680, August 1981, pp 1 - 18 (N82-17123)

16. Abstract

A quantitative evaluation method of the suction effect from a suction plate on side walls is explained. It is found from wind tunnel tests that the wall interference is basically described by the summation form of wall interference in the case of two dimensional flow and the interference of side walls.

17. Key Words (Selected by Author(s))	18. Distribution Statement
	Unclassified and Unlimited

19. Security Classif. (of this report)	20. Security Classif. (of this page)	21. No. of Pages	22. Price
Unclassified	Unclassified	39	

A NEW METHOD OF EVALUATING THE SIDE WALL INTERFERENCE EFFECT ON AIRFOIL ANGLE OF ATTACK BY SUCTION FROM THE SIDE WALLS*

Hideo Sawada, Seizo Sakakibara, Mamoru Sato, Hiroshi Kanda, Toshio Karasawa**

1. Preface

Interference from the walls of a two-dimensional wind /1*** tunnel is generally treated as being identical on a flat surface where the flow in the test section is in an arbitrary position and is parallel to the side walls. However, the actual flow area which is created in the test section is not flat. The space between the side walls in the test section of the wind tunnel, which is called a two-dimensional wind tunnel and the wind tunnel which was made for testing only airfoil models, is very narrow compared to its height. Thus it is natural to consider that the flow area in the test section is completely different from the flat one. If the width of the test section /2 is wide enough, the flow area which is created inside approaches the flatter one. Here the width of the test section is very narrow compared to its height (ratio of height to width is greater than 2), so we shall call the wind tunnel for testing only the two- dimensional model a two-dimensional wind tunnel.

One of the wind tunnel wall interferences which will become important for the two-dimensional wind tunnel is side wall interference. Since this has a narrow space between the side walls, the boundary layer which was developed on the walls has a strong influence on the region which is considered as the

---

* Report published August 1981
** National Aerospace Laboratory
*** Numbers in margin indicate foreign pagination

flow potential formed in the test section. Because of that, the flow area in the test section does not become two dimensional; therefore, this phenomenon is called side wall interference. It is very difficult to evaluate the influence on flow potential in the boundary layer which develops on the side walls. For example, at a junction of two dimensional model and the side walls, there is a very complex three dimensional boundary layer. It is currently still impossible to predict the motion of a viscous fluid there accurately. Therefore, as far as the writers know, evaluation of the amount of side wall interference has been impossible until now. Except in the cases that the lift of the airfoil model was large or a shock wave occurred on the airfoil, it is known from experience that the amount of side wall interferences is small. When the space between the side walls is extremely small compared to the height of the test section, it was reported that the amount of side wall interference becomes large, so it must be evaluated.[1]

In the two dimensional wind tunnel where the performance of airfoil models at high subsonic speed is tested, a suction plate is installed in a portion of the side walls around the model in order to prevent the shock wave from bending toward the span direction. [2,3] In the conditions under which the suction plate is installed, fluid in the test section can go in and out of the test section through the suction plate to some degree. Also, the amount can be changed by adjusting the pressure bleed chamber on the side of the suction plate. Experimentally it is known that, if the amount of fluid suction in the test section through the suction plate is increased, the lift which occurs in the airfoil model matrix increases [4]. Therefore, even at the same flow velocity and at the same angle of attack setting, different lift coefficients are obtained at different amounts of suction. It is currently difficult to determine which lift coefficient of which amount of suction is the real lift coefficient of a two dimensional airfoil model.

Considering the present conditions, the writers have already reported a method of handling wall interference of a two dimensional wind tunnel as wall interference of a three dimensional wind tunnel [5]. Using this method, in this report, we are going to explain the quantitative evaluation method of the suction effect from a suction plate on the side walls.

2. Analysis

The most important thing at the time of quantitative evaluation of wind tunnel wall interference is that it is necessary to decide beforehand about what is the case of no interference. In this report, we are going to follow a report which has been written by these writers and has been publicly presented already [5]. Namely, the following concern the flow area which does not have wall interference and the airfoil model matrix in it.

(1) The condition of homogeneity is the same as the one of the wind tunnel.

(2) Although the width distribution of the airfoil model is the same as the airfoil model which was used for the wind tunnel test, the length of the span direction of airfoil model matrix is infinite. Therefore, the circulation distribution which occurs on the airfoil model matrix is invariant toward span direction.

(3) The circulation distribution of airfoil chord length direction agrees with the one on the central sectional surface of the airfoil model matrix in the wind tunnel test.

On the other hand, when there is a homogeneous airfoil which spreads out infinitely, if the minute disturbance potential $\tilde{\phi}$ follows [5], the following will be described.

$$\tilde{\phi}(x,y,z) = -\iint_{S_{wing}} S(\xi,\eta)\cdot\tilde{\Psi}_\zeta|_{\zeta=0}\,d\xi d\eta$$

$$-\iint_{S_w} [\tilde{\phi}]^{\pm}\cdot\tilde{\Psi}_\zeta|_{\zeta=0}\,d\xi d\eta \qquad (1)$$

Here, $\tilde{\phi}$ will be defined as follows.

$$\begin{cases} \tilde{\Phi} = U_\infty\cdot(\hat{x}+\tilde{\phi}) & (2)\\ \tilde{\phi} = \beta^2\cdot\tilde{\Phi} & (3)\\ (x,y,z) = (\xi,\eta,\zeta) = (\hat{x},\beta\hat{y},\beta\hat{z}) & (4)\\ \beta = \sqrt{1-M_\infty^2} & (5) \end{cases}$$

Also,

$$-\frac{1}{4\pi}\cdot\frac{1}{\sqrt{(\xi-x)^2+(\eta-y)^2+(\zeta-z)^2}} \qquad (6)$$

From the basic condition [2], equation [1] will be transformed furthermore

$$\tilde{\phi}(x,y,z) = -\frac{1}{2\pi}\int_{x_L}^{x_T}\frac{\xi-x}{(\xi-x)^2+z^2}S_2(\xi)d\xi$$

$$+\frac{1}{2\pi}\int_{x_L}^{\infty}\frac{z}{(\xi-x)^2+z^2}[\hat{\phi}]^{\pm}\,d\xi \qquad (7)$$

/3

and it is understood that η does not change toward $\tilde{\phi}$ direction, namely the span direction. However, in the wind tunnel the minute disturbance potential of flow area which occurs from the airfoil model matrix is three dimensional. According to [5]

$$\phi(x,y,z) = -\iint_{S_{wing}} S(\xi,\eta)\cdot\Psi_\zeta|_{\zeta=0}\,d\xi d\eta$$

$$-\iint_{S_w} [\phi]^{\pm}\cdot\Psi_\zeta|_{\zeta=0}\,d\xi d\eta$$

$$-\iint_{Y}\{u\cdot g+v\cdot\Psi\}_{-L}^{L}d\xi d\zeta$$

$$-\iint_{Z}[u\cdot h+w\cdot\Psi]_{-H}^{H}\,d\xi d\eta \qquad (8)$$

Here, ϕ is defined to be the same as $\tilde{\phi}$ as follows:

$$\begin{cases} \Phi = U_\infty(\hat{\phi}+\hat{x}) & (9) \\ \phi = \beta^2\hat{\phi} & (10) \end{cases}$$

Also

$$\begin{aligned} \Psi = {} & \frac{1}{8HL}|\xi-x| - \frac{1}{4\pi H}\sum_{m=1}^{\infty}\frac{1}{m}e^{-\frac{m\pi}{L}|\xi-x|} \\ & \times\cos\frac{m\pi}{L}(\eta-y) \\ & -\frac{1}{4\pi L}\sum_{n=1}^{\infty}\frac{1}{n}\cdot e^{-\frac{n\pi}{H}|\xi-x|}\cdot\cos\frac{n\pi}{H}(\zeta-z) \\ & -\frac{1}{2HL}\sum_{n=1}^{\infty}\sum_{m=1}^{\infty}\frac{1}{k}\cdot e^{-k|\xi-x|}\cdot\cos\frac{m\pi}{L}(\eta-y) \\ & \times\cos\frac{n\pi}{H}(\zeta-z) \end{aligned} \qquad (11)$$

Here,

$$k = \pi\sqrt{\left(\frac{n}{H}\right)^2+\left(\frac{m}{L}\right)^2} \qquad (12)$$

Also, the domains S_{wing}, S_W are shown in Figure 2 and the domains Y, Z are the test surface. Namely,

$$\iint_Y d\xi d\zeta = \int_{-\infty}^{\infty} d\xi \int_{-H}^{H} d\zeta \qquad (13)$$

$$\iint_Z d\xi d\eta = \int_{-\infty}^{\infty} d\xi \int_{-L}^{L} d\eta \qquad (14)$$

Also,

$$\{\mathcal{M}(\xi,\eta,\zeta)\}_{-L}^{L} = \mathcal{M}(\xi,L,\zeta) - \mathcal{M}(\xi,-L,\zeta) \qquad (15)$$

$$[\mathcal{M}(\xi,\eta,\zeta)]_{-H}^{H} = \mathcal{M}(\xi,\eta,H) - \mathcal{M}(\xi,\eta,-H) \qquad (16)$$

Figure 1. Wind tunnel test section.

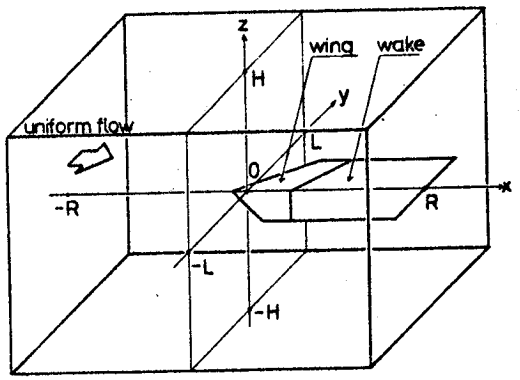

Figure 2. S_{wing} and S_{wake}

/4

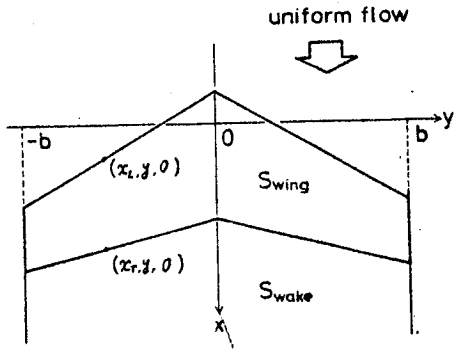

$$[\mathcal{M}(\xi,\eta,\zeta)]_{-}^{+} = \lim_{\epsilon \to +0} \{\mathcal{M}(\xi,\eta,\epsilon) - \mathcal{M}(\xi,\eta,-\epsilon)\} \tag{17}$$

$$g = -\int_{\ell}^{\infty} \frac{\partial \Psi}{\partial \eta}\, d\xi \tag{18}$$

$$h = -\int_{\ell}^{\infty} \frac{\partial \Psi}{\partial \zeta}\, d\xi \tag{19}$$

Figure 3 shows the coordinates, etc. of a test section of a two dimensional wind tunnel.

Figure 3. Test section of two dimensional wind tunnel.

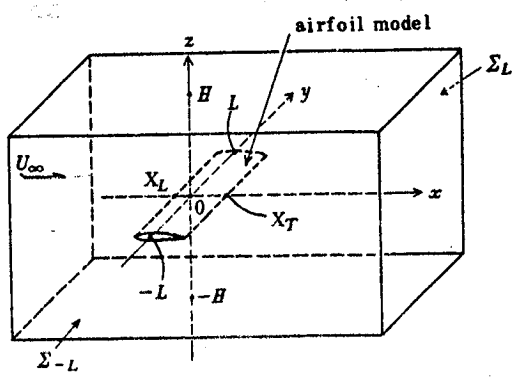

The width distribution of an airfoil model matrix is invariant toward span direction, so equation (8) will be as follows:

$$\phi(x,y,z) = -\frac{1}{2\pi}\int_{x_L}^{x_T} S_2(\xi) \times \sum_{n=-\infty}^{\infty} \frac{\xi - x}{(2nH+z)^2+(\xi-x)^2}\, d\xi - \int_{x_L}^{\infty} d\xi \int_{-L}^{L} (\phi)^{\pm} \cdot \Psi_\zeta|_{\zeta=0}\, d\eta - \iint_Y \{u\cdot g + v\cdot \Psi\}_{-L}^{L}\, d\xi d\zeta - \iint_Z (u\cdot h + w\cdot \Psi)_{-H}^{H}\, d\xi d\eta \qquad (20)$$

Here, wind tunnel wall interference potential φ is defined as a difference from minute disturbance potential $\phi(x,0,z)$ of the wind tunnel central cross section and $\tilde{\phi}(x,y,z)$ of free flow. Namely,

$$\varphi(x,z) = \tilde{\phi}(x,y,z) - \phi(x,0,z) \qquad (21)$$

$\varphi(x,z)$ will be described as follows by the positive forms of equations (7), (20), and (21).

$$\varphi(x,z) = \frac{1}{2\pi}\int_{x_L}^{x_T} S_2(\xi)\cdot \sum_{n=1}^{\infty} \left[\frac{\xi - x}{(2Hn+z)^2+(\xi-x)^2} + \frac{\xi - x}{(2Hn-z)^2+(\xi-x)^2}\right] d\xi + \int_{x_L}^{\infty} d\xi \left[\int_{-L}^{L} (\phi)^{\pm}\cdot \Psi_\zeta(\xi,\eta,0;x,0,z)\, d\eta + \frac{1}{2\pi}\cdot\frac{z}{(\xi-x)^2+z^2}(\tilde{\phi})^{\pm}\right] + \iint_Y \{u\cdot g + v\cdot \Psi\}_{-L}^{L}\, d\xi d\zeta + \iint_Z (u\cdot h + w\cdot \Psi)_{-H}^{H}\, d\xi d\eta \qquad (22)$$

Therefore, $\varphi_x(x,\pm 0), \varphi_z(x,\pm 0)$, which corresponds to the increment of the velocity component in the x, z direction by interference from wind tunnel walls on the airfoil surface $(z\to\pm 0)$, is as follows:

$$\varphi_x(x,\pm 0)=\frac{1}{2\pi}\int_{x_L}^{x_T} S_2(\xi)$$

$$\times\left\{\frac{\pi^2}{4H^2}\operatorname{cosech}^2\frac{\pi}{2H}(\xi-x)-\frac{1}{(\xi-x)^2}\right\}d\xi$$

$$-\sum_{n=0}^{\infty}\int_{-\infty}^{\infty} v_{LC}^{a(n)}(\xi)\cdot J_B^{(n)}\left(\frac{\xi-x}{L};\lambda\right)d\left(\frac{\xi}{L}\right)$$

$$-\sum_{m=0}^{\infty}\int_{-\infty}^{\infty} w_{HC}^{a(m)}(\xi)\, J_B^{(m)}\left(\frac{\xi-x}{H};\frac{1}{\lambda}\right)d\left(\frac{\xi}{H}\right) \qquad (23)$$

/5

Here,

$$J_B^{(n)}(x;\lambda)=\begin{cases}\dfrac{1}{4}\tanh\left(\dfrac{\pi}{2}x\right) & \text{for } n=0\\[2ex] \dfrac{2n}{\lambda}\displaystyle\sum_{\nu=1}^{\infty}\frac{x}{\sqrt{(2\nu-1)^2+x^2}}\\[2ex] \quad\times K_1\left(\dfrac{n\pi}{\lambda}\sqrt{(2\nu-1)^2+x^2}\right)\end{cases}$$

$$\text{for } n=1,2,3,\ \cdots\cdots \qquad (24)$$

$$\lambda=H/L \qquad (25)$$

Figure 4 and 5 show a picture of $J_B^{(n)}(x;\lambda)$ in terms of x. Also, $v_{LC}^{a(n)}$, $w_{LC}^{a(m)}$ is the following quantity.

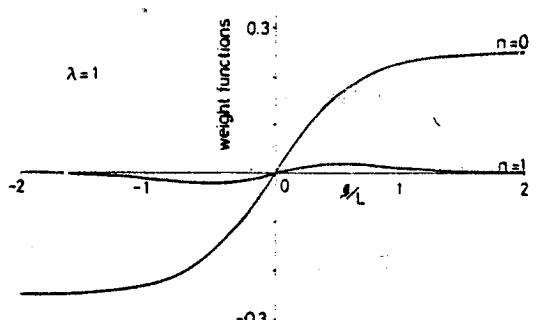

Figure 4. $J_B^{(n)}\left(\frac{\xi}{L};1\right)$

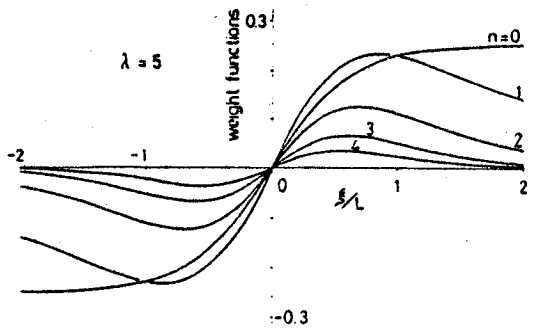

Figure 5. $f_B^{(n)}(\frac{\xi}{L};5)$

$$v_{LC}^{a(n)}=\frac{1}{2H}\int_{-H}^{H}\{v(\xi,L,\zeta)-v(\xi,-L,\zeta)\}$$

$$\times\cos\frac{n\pi}{H}\zeta\,d\zeta \qquad (n=0,1,2,\cdots\cdots) \tag{26}$$

$$w_{HC}^{a(m)}=\frac{1}{2L}\int_{-L}^{L}\{w(\xi,\eta,H)-w(\xi,\eta,-H)\}$$

$$\times\cos\frac{m\pi}{L}\eta\,d\eta \qquad (m=0,1,2,\cdots\cdots) \tag{27}$$

Figure 6 shows $v_{LC}^{a(n)}, w_{HC}^{a(m)}$ which is approximately the representative case.

$$\varphi_z(x,\pm 0)=\int_{x_L}^{\infty}d\xi$$

$$\Big[\int_{-L}^{L}(\phi)_{-}^{+}\cdot\Psi_{\zeta z}(\xi,\eta,o\,;x,o,\pm o)\,d\eta$$

$$+\frac{1}{2\pi}\cdot\frac{1}{(\xi-x)^2}(\tilde{\phi})_{-}^{+}\Big]$$

$$-\sum_{m=0}^{\infty}\int_{-\infty}^{\infty}u_{HC}^{a(m)}(\xi)\cdot f_U^{(m)}\Big(\frac{\xi-x}{H};\lambda\Big)d\Big(\frac{\xi}{H}\Big)$$

$$-\sum_{n=1}^{\infty}\int_{-\infty}^{\infty}v_{LS}^{a(n)}(\xi)\cdot f_V^{(n)}\Big(\frac{\xi-x}{L};\lambda\Big)d\Big(\frac{\xi}{L}\Big) \tag{28}$$

Here,

$$f_V^{(n)}(x;\lambda)=\frac{2n}{\lambda}\sum_{\nu=1}^{\infty}K_0\Big(\frac{n\pi}{\lambda}\sqrt{(2\nu-1)^2+x^2}\Big) \tag{29}$$

for $n=1,2,3,\cdots\cdots$

$$J_U^{(m)}(x;\lambda)=\begin{cases}\dfrac{1}{2}\cdot\dfrac{1}{1+e^{\pi x}} & \text{for } m=0,\\ m\pi\lambda\,\mathrm{cosech}\,(m\pi\lambda)\cdot\mathbb{1}(-x)+\dfrac{1}{2}\mathrm{sgn}\,(x)\cdot e^{-m\pi\lambda|x|}\\ \quad+\mathrm{sgn}\,(x)\cdot m^2\lambda^2\sum_{n=1}^{\infty}\dfrac{(-1)^n}{n^2+\lambda^2m^2}\\ \quad\times e^{-\pi\sqrt{n^2+\lambda^2m^2}\cdot|x|}\\ \quad-2m\lambda x\sum_{\nu=1}^{\infty}\dfrac{1}{\sqrt{(2\nu-1)^2+x^2}}\\ \quad\times K_1\left(m\pi\lambda\sqrt{(2\nu-1)^2+x^2}\right)\\ \quad\text{for } m=1,2,3,\cdots\cdots\end{cases}\tag{30}$$

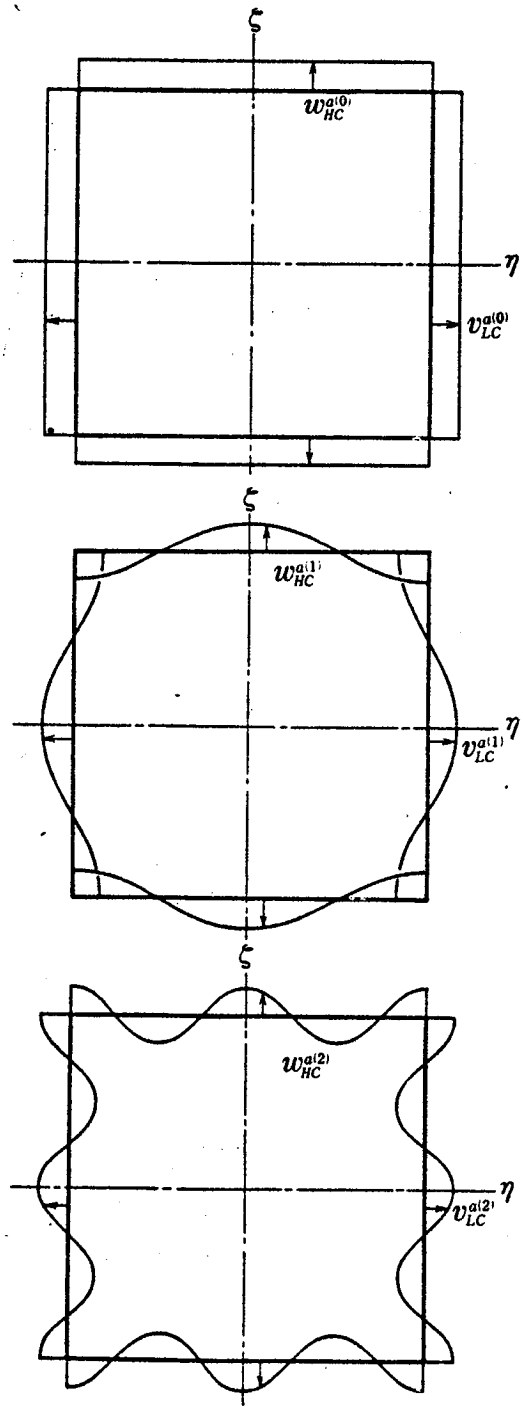

/6

Figure 6. $w_{HC}^{a(n)}$ and $v_{LC}^{a(n)}$ $(n=0,1,2)$

Figure 7 and 8 show a picture of $J_V^{(n)}(x;\lambda)$, $J_U^{(m)}(x,\lambda)$ in terms of x. Also, $u_{HC}^{a(m)}$, $v_{LS}^{a(n)}$ is the following quantity.

$$u_{HC}^{a(m)} = \frac{1}{2L}\int_{-L}^{L}\{u(\xi,\eta,H)-u(\xi,\eta,-H)\}$$

$$\times\cos\frac{m\pi}{L}\eta\, d\eta \qquad m=0,1,2,\cdots\cdots \tag{31}$$

Figure 7.1. $J_V^{(n)}(\frac{\xi}{L};1)$

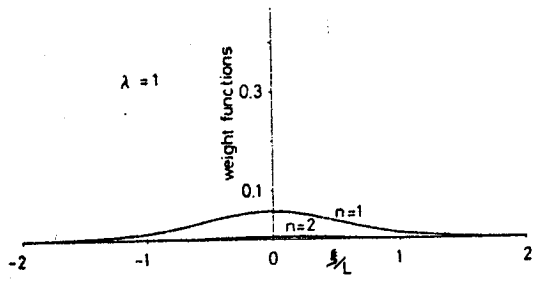

Figure 7.2. $J_V^{(n)}(\frac{\xi}{L};5)$

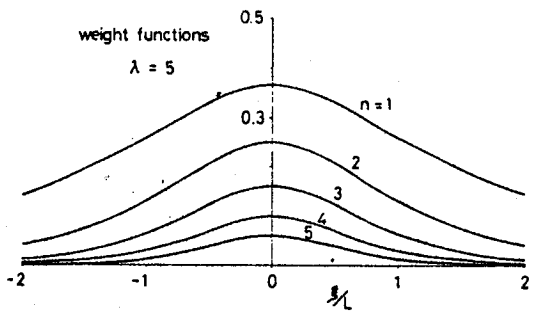

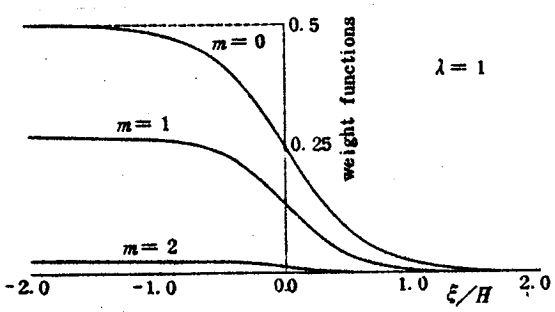

Figure 8.1. $J_U^{(m)}(\frac{\xi}{H};1)$

Figure 8.2. $J_U^{(m)}\left(\frac{\xi}{H};5\right)$

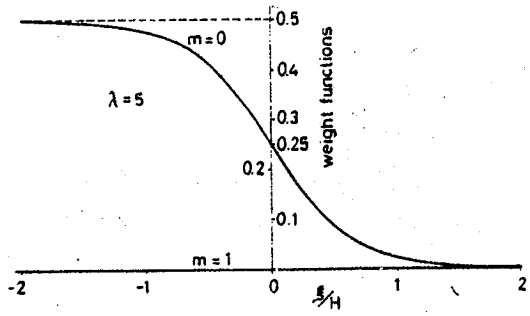

$$v_{LS}^{a(n)} = \frac{1}{2H}\int_{-H}^{H}\{v(\xi,L,\zeta)-v(\xi,-L,\zeta)\}$$

$$\times \sin\frac{n\pi}{H}\zeta\, d\zeta \qquad n=1,2,3,\cdots\cdots \qquad (32)$$

Figure 9 and 10 show the representative case of $u_{HC}^{a(m)}, v_{LS}^{a(n)}$.

From the characteristics of $J_B^{(n)}(x;\lambda)$ if λ is small, toward at $n\geq 1$, $J_B^{(n)}$ is very small toward $J_B^{(o)}$. Consequently, the term which affects $J_B^{(n)}(x;\lambda)$ $(n\geq 1)$ can be ignored compared to the other terms. As known from equation (25), λ is large in the usualy two dimensional wind tunnel; therefore, we can approximate equation (23) accurately as follows:

$$\varphi_x(x,\pm 0)\simeq \frac{1}{2\pi}\int_{x_L}^{x_T} S_2(\xi)\cdot\left\{\frac{\pi^2}{4H^2}\operatorname{cosech}^2\frac{\pi}{2H}(\xi-x)\right.$$

$$\left.-\frac{1}{(\xi-x)^2}\right\}d\xi$$

$$-\frac{1}{4H}\int_{-\infty}^{\infty} w_{HC}^{a(o)}\cdot\tanh\left(\frac{\pi}{2H}(\xi-x)\right)d\xi$$

$$-\sum_{n=0}^{N_B}\int_{-\infty}^{\infty} v_{LC}^{a(n)}(\xi)\cdot J_B^{(n)}\left(\frac{\xi-\lambda}{L};\lambda\right)d\left(\frac{\xi}{L}\right) \qquad (23)$$

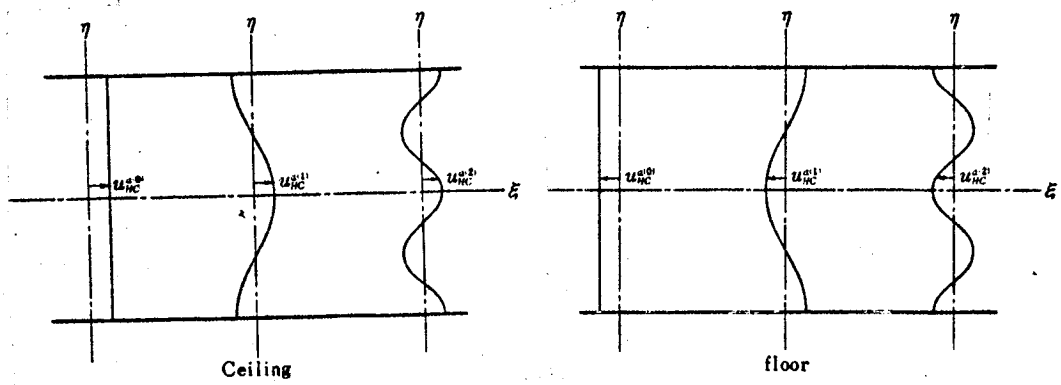

Figure 9. $u_{HC}^{a(m)}(m=0,1,2)$

Here, N_B is a large positive integer.

The 1st and 2nd terms of the right side of equation (23)' describe the amount of barrage interference in the two dimensional case obtained when the flow potential which is formed in test section is completely flat. The 3rd term on the right side of equation (23)' describes the influence that suction of fluid in the test section from side walls exerts on the flow potential formed in the test section. Therefore, if this term is evaluated quantitatively, it means that the amount of interference which corresponds to the x direction velocity increment in the side wall interference effect was evaluated.

/8

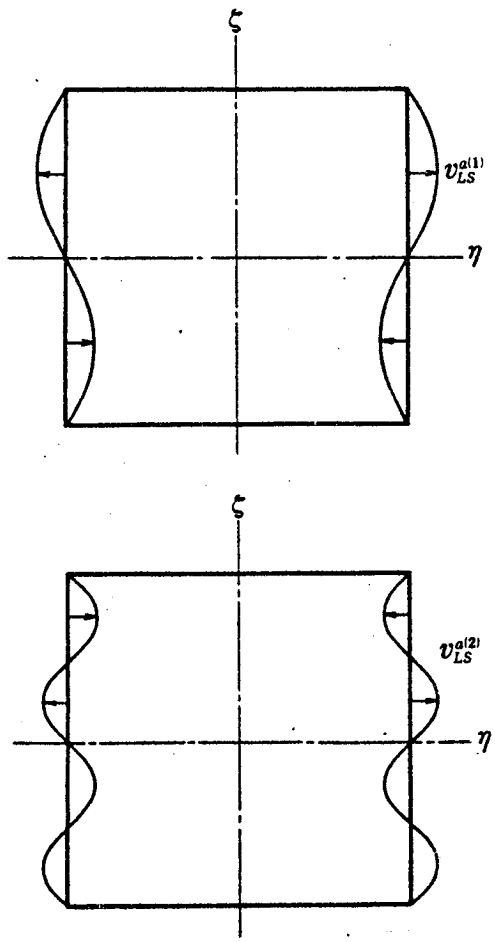

Figure 10. $v_{LS}^{a(n)}$ ($n=1,2$)

On the other hand, from the characteristics of $J_U^{(m)}(x;\lambda)$ if λ is large, the value is extremely small at $m \geq 1$, and it is understood that $u_{HC}^{a(m)}$ $(m \geq 1)$ has almost no influence on the value of the right side of equation (28). Therefore, equation (28) can be approximated as follows in the two dimensional wind tunnel.

$$\varphi_z(x,\pm 0) \simeq \int_{x_L}^{\infty} \Big[\int_{-L}^{L} (\phi)^{\pm} \cdot \Psi_{tz}(\xi,\eta,0;x,0,\pm 0)\, d\eta + \frac{1}{2\pi} \cdot \frac{1}{(\xi-x)^2} (\tilde{\phi})^{\pm} \Big] d\xi - \frac{1}{2H} \int_{-\infty}^{\infty} \frac{u_{HC}^{a(0)}}{1+e^{\frac{\pi}{H}(\xi-x)}}\, d\xi - \sum_{n=1}^{N_L} \int_{-\infty}^{\infty} v_{LS}^{a(n)} \cdot J_V^{(n)}\left(\frac{\xi-x}{L};\lambda\right) d\left(\frac{\xi}{L}\right) \qquad (28)'$$

Here, N_L is a large natural number. The first term on the right side of equation (28)' describes the interference effect in the case when circulation distribution of airfoil model matrix in wind tunnel changes in the span direction. The 2nd term describes the interference effect from upper and lower walls of the test section when the potential flow area in the test section is completely two dimensional. The 3rd term describes the amount of interference which corresponds to the increment in the z directional velocity component of the side wall interference effect.

How, for simplicity we assume that the pressure distribution of the airfoil model between both side walls becomes constant with the proper suction from the side walls. This was confirmed from the experiemental fact that even if the amount of suction from the side walls is changed somewhat, the pressure distribution of the airfoil model is constant in the span direction. (refer to Figure 11). We are going to limit our statements in the following discussion only to the cases when this kind of assumption

is realized. Since $(\phi)^{\pm}$ is invariant in the y direction, equation (28)' is further adjusted and it will become

$$\varphi_z(x,\pm 0) \simeq \frac{1}{4H}\int_{x_L}^{x_T} (u)^{\pm} \cdot d\xi$$

$$+\frac{1}{2AH^2}\int_{x_L}^{x_T} (u)^{\pm} \cdot (x-\xi)\, d\xi$$

$$-\frac{1}{2H}\int_{-\infty}^{\infty} \frac{u_{HC}^{a(o)}}{1+e^{\frac{\pi}{H}(\xi-x)}} d\xi$$

$$-\sum_{n=1}^{N_L}\int_{-\infty}^{\infty} v_{LS}^{a(n)} \cdot J_V^{(n)}\left(\frac{\xi-x}{L};\lambda\right) d\left(\frac{\xi}{L}\right) \qquad (28)''$$

All of the right hand 1st, 2nd, and 3rd terms in the above equation exhibit two dimensional lift interference.

From the above, in the case when an airfoil model test is performed with the two dimensional wind tunnel, if the proper suction is performed from the side walls, and the pressure distribution of airfoil model matrix is made constant in the span direction, wall interference of the wind tunnel test section /9 will be described by equation (23)' and (28'') as the usual two dimensional wall interference and the interference by suction from the side walls.

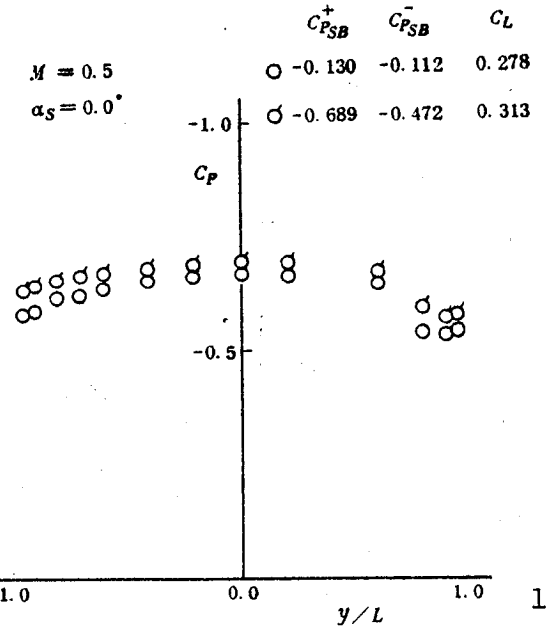

Figure 11. Pressure distribution from leading edge to airfoil top face of 40% airfoil chord length in the span direction.

3. Evaluation of the influence on the effective angle of attack on an airfoil model by suction from the side walls.

The test surfact, which is flat and parallel to the side walls, and which exists outside of the boundary layer created on side walls and which is crossed by the 7-axis at the points L, -L, is made Σ_L, Σ_{-L} . Until the last section (Figure 3) it was understood that the side wall interference of a two dimensional wind tunnel can be evaluated if the distribution of the velocity component perpendicular to the test surface is known. The boundary layer which developed on side walls influences its outside flow potential. It is possible to evaluate the influence if the velocity component which is perpendicular to this surface is measured on Σ_L, Σ_{-L} . However, in fact, measuring this velocity component over the surface is difficult. In the case when flow of uniform Mach number and the airfoil model angle of attack are low, as they do not form a supersonic domain and large separation area on the airfoil surface, the side wall interference effect on a two dimensional wind tunnel by the boundary layer which is created on the side walls of this kind of solid has been ignored except in the case when the space between the side walls is exremely narrow compared to the height of the test section. (for example, H/L = 5). Because of this reason we will not discuss the influence of the boundary layer which occurs at the solid wall section of the side walls; we will only discuss the influence in the case of a suction boundary layer on the side walls through a suction plate. Especially, it is understood from the discussion in the previous section that $\varphi_z(x, \pm 0)$ on the x axis introduced from the influence of the boundary layer becomes

$$-\sum_{n=1}^{N_L} \int_{-\infty}^{\infty} v_{LS}^{a(n)} \cdot J_V^{(n)}\left(\frac{\xi - x}{L}; \lambda\right) d\left(\frac{\xi}{L}\right) \qquad (28)'''$$

from equation (28)''.

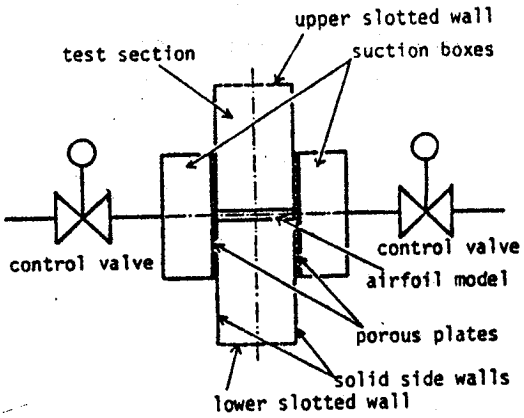

Figure 12. Suction mechanisms from side walls.

The fluid suction method in the test section is considered here as a method shown in Figure 12. This is a suction method which is employed in the two dimensional wind tunnel of the National Aerospace Laboratory. [4] As understood from the figure, control of the amount of suction is achieved by controlling the pressure in a box called a suction box by properly adjusting the degree of opening of the valve for controlling suction amount. Here, the influence of the pressure change in this suction box on v(x,L,z) and v(x,-L, z); namely, the influence on the velocity component perpendicular to the test surface at Σ_L, Σ_{-L} , which is the test surface near the side walls, can be approximated if the static pressure at the point of (x ± L, z) in the test section is proportional to the square root of the pressure difference with the pressure in the suction box. This approximation is used widely for the aerodynamic characteristics of a porous wall. Although this does not always describe a highly accurate approximation, it is known that the basic characteristics are sufficiently described [2].

$$P - P_{SB} = K \cdot \frac{1}{2} \rho_\infty v_n^2 \qquad (33)$$

Here, ρ_∞ is density of a uniform flow wind tunnel, v_n is the velocity component perpendicular to the suction plate, p is the lateral pressure of test section of the suction plate,

P_{SB} is the suction box pressure, and K is a constant which is called the suction plate pressure loss coefficient. It is known that this pressure coefficient is not always constant [4], but it is constant for large change of p. The change at the position of the static pressure in the flow area around air foil model is almost of the degree of dynamic pressure except for the area very close to the airfoil surface. Therefore, in the case when fluid in the test section is sucked by using a suction plate near the airfoil model matrix, it does not matter if the pressure loss coefficient is constant. If both sides of equation (33) are divided by the uniform flow dynamic pressure

$$C_P - C_{P_{SB}} = K \cdot \left(\frac{v_n}{U_\infty}\right)^2 \tag{34}$$

Here, U_∞ is a uniform flow velocity

$$C_P = \frac{P - P_\infty}{\frac{1}{2}\rho_\infty U_\infty^2} \tag{35}$$

$$C_{P_{SB}} = \frac{P_{SB} - P_\infty}{\frac{1}{2}\rho_\infty U_\infty^2} \tag{36}$$

Here, P_∞ is a uniform flow static pressure.

Since the direction of v_n' is toward low pressure, equation (34) is rewritten as follows:

$$\frac{v_n}{U_\infty} = \mathrm{sgn}(C_P - C_{P_{SB}}) \cdot \frac{1}{\sqrt{K}} \sqrt{|C_P - C_{P_{SB}}|} \tag{37}$$

where the direction which is decided as positive is from the inside of the test section outward through the suction plate. Figure 13 is a figure looking upstream from the downstream side of the two dimensional wind tunnel. In the case when the fluid inside of the test section flows out, the sign of the velocity component perpendicular to the wall is positive. On the other hand, when fluid flows out after going through the suction plate on the left side, the sign becomes negative. Now, if the pressure coefficient, which is defined by equation (36) of the pressure

in the right side suction box, is set as $C_{P_{SB}}^{+}$, , and the pressure coefficient in left side is set as $C_{P_{SB}}^{-}$

$$v_n(x,L,z) = \mathrm{sgn}(C_P - C_{P_{SB}}^{+}) \cdot \kappa \sqrt{|C_P - C_{P_{SB}}^{+}|} \tag{38}$$

$$v_n(x,-L,z) = -\mathrm{sgn}(C_P - C_{P_{SB}}^{-}) \cdot \kappa \sqrt{|C_P - C_{P_{SB}}^{-}|} \tag{39}$$

Here, k is

$$\kappa = 1/\sqrt{K} \tag{40}$$

On the other hand, from equation (9) and (10) which are definition equations of the minute disturbance potential ϕ, , $v(x, \pm L, z) = \beta \cdot v_n(x, \pm L, z)$ (double signs are in the same order) (41).

Here,

$$v = \phi_z \tag{42}$$

Therefore,

$$v(x,L,z) = \mathrm{sgn}(C_P - C_{P_{SB}}^{+}) \cdot \beta\kappa \cdot \sqrt{|C_P - C_{P_{SB}}^{+}|} \tag{38}'$$

$$v(x,-L,z) = -\mathrm{sgn}(C_P - C_{P_{SB}}^{-}) \cdot \beta\kappa \cdot \sqrt{|C_P - C_{P_{SB}}^{-}|} \tag{39}'$$

If v of equations (38)' and (39)' are substituted in equation (32),

$$v_{LS}^{a(n)} = \frac{1}{2H}\int_{-H}^{H} \beta\kappa \cdot \mathrm{sgn}(C_P - C_{P_{SB}}^{+}) \cdot \sqrt{|C_P - C_{P_{SB}}^{+}|} \times \sin\frac{n\pi}{H}\zeta \, d\zeta + \frac{1}{2H}\int_{-H}^{H} \beta\kappa \cdot \mathrm{sgn}(C_P - C_{P_{SB}}^{-}) \times \sqrt{|C_P - C_{P_{SB}}^{-}|} \cdot \sin\frac{n\pi}{H}\zeta \, d\zeta$$

$$n = 1, 2, 3, \cdots\cdots \tag{43}$$

Here, we will define the amount of $v_{LS}^{a(n)+}$, $v_{LS}^{a(n)-}$

$$v_{LS}^{a(n)+}=\frac{\beta\kappa}{H}\int_{-H}^{H}\mathrm{sgn}(C_P-C_{P_{SB}}^{+})\cdot\sqrt{|C_P-C_{P_{SB}}^{+}|}\times\sin\frac{n\pi}{H}\zeta\,d\zeta \tag{44}$$

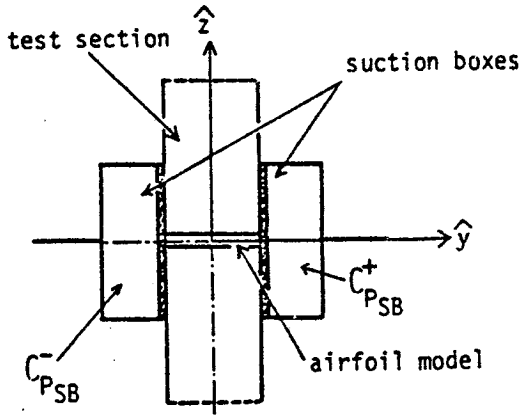

Figure 13. $C_{P_{SB}}^{+}$ と $C_{P_{SB}}^{-}$

$$v_{LS}^{a(n)-}=\frac{\beta\kappa}{H}\int_{-H}^{H}\mathrm{sgn}(C_P-C_{P_{SB}}^{-})\cdot\sqrt{|C_P-C_{P_{SB}}^{-}|}\times\sin\frac{n\pi}{H}\zeta\,d\zeta \tag{45}$$

/11

If $v_{LS}^{a(n)}$ is described by using $v_{LS}^{a(n)+}$, $v_{LS}^{a(n)-}$

$$v_{LS}^{a(n)}=\frac{1}{2}\{v_{LS}^{a(n)+}+v_{LS}^{a(n)-}\} \tag{46}$$

Therefore, if the amount which corresponds to an increment of the velocity component in the z direction of the side wall interference described by (28)''' is described by $\varphi_z^*(x,\ \pm 0)$

$$\varphi_z^*(x,\pm 0)=\frac{1}{2}\Big[-\sum_{n=1}^{N_L}\int_{-\infty}^{\infty}v_{LS}^{a(n)+}\times J_V^{(n)}\Big(\frac{\xi-x}{L};\lambda\Big)d\Big(\frac{\xi}{L}\Big)-\sum_{n=1}^{N_L}\int_{-\infty}^{\infty}v_{LS}^{a(n)-}\cdot J_V^{(n)}\Big(\frac{\xi-x}{L};\lambda\Big)d\Big(\frac{\xi}{L}\Big)\Big] \tag{47}$$

As understood from equations (44) and (45), $v_{LS}^{a(n)+}$ is equal to the case of $v_{LS}^{a(n)}$ which was made by some method to become equal to the pressure in the suction box located on the left side of Figure 13. $v_{LS}^{a(n)-}$ is also $v_{LS}^{a(n)}$ when the suction pressure in right side is made equal to that of the left side. Because of that reason, $\varphi_z^*(x,\pm 0)$ described in equation (47) describes the average amount of suction interference from the side walls which is found when the pressure in one of the two suction boxes enters both suction boxes; and, on the other hand, the interference amount which is found when the pressure in the other suction box enters both of the suction boxes. And, it means that the amount of side wall interference by suction is described when different pressures enter the two suction boxes. Definitely, for the fluid suction process in the test section from usual side walls, it is attempted to make the inside pressure of both of the suction boxes possibly become equal. However, as in the two dimensional wind tunnel of the National Aerospace Technical Laboratory, in the case when the left and right side suction systems are separated, the internal pressure of both of the suction boxes cannot agree completely. However, it is understood that this case also can be evaluated sufficiently if equation (47) is used.

From the above discussion if $C_p(x,\pm L,z)$ is measured on suction plate, and $C_{P_{SB}}^+, C_{P_{SB}}^-$ is also measured at the same time, it is understood from equation (47) that an increment $\varphi_z^*(x,\pm 0)$ of the z directional velocity component in the amount of side wall interference from suction is found. However, as understood from equations (44) and (45), an undetermined k is still included in $\varphi_z^*(x,\pm 0)$. Strictly speaking if $/C_p, C_{P_{SB}}^+, C_{P_{SB}}^-/$ is defined $/\varphi_z^*(x,\pm 0)/$ is simply determined. k can be uniquely dtermined beforehand from other experiment, but under the conditions where a uniform flow runs is test section, a boundary layer develops on the suction plate and k must be determined for various cases. Because of that we will state the method in this report

that even if the value of k is now known, the suction effect will be known as follows. If $\varphi_z^*(x,\pm 0)$ is obtained from equation (47), the upwash distribution from suction on x-axis becomes

$$-\frac{1}{\beta}\varphi_z^*(x,\pm 0) \tag{49}$$

An increment $\Delta\alpha_S$ of the effective angle of attack of the airfoil model corresponding to this upwash distribution is

$$\Delta\alpha_S = -\frac{1}{c\beta}\int_{x_L}^{x_T}\varphi_z^*(x,\pm 0)\,dx \tag{50}$$

[6]. How, $\Delta\alpha_S^*$ is defined as follows:

$$\Delta\alpha_S^* = \Delta\alpha_S/\kappa \qquad (\kappa \neq 0) \tag{51}$$

As mentioned before, , $\Delta\alpha_S$ is not determined unless k has been determined. On the other hand, from equation (51), regardless of k, $\Delta\alpha_S^*$ is the amount to be determined if $C_P, C_{P_{SB}}^+, C_{P_{SB}}^-$ is known. Now, assuming that the proper amount of suction from the side walls are performed, $\Delta\alpha_S^*$ becomes 0. At this time $\Delta\alpha_S$ also becomes 0 no matter how much the k values from equation (51) are. Namely, if suction from side walls is adjusted for $\Delta\alpha_S^*$ to become 0, no change in the effective angle of attack of airfoil model with suction occur. But, during the experiment it is considered that it is difficult to adjust the amount of suction by calculating $\Delta\alpha_S^*$ in order for the value to become 0. Therefore, in the case when a portion of fluid in the test section is sucked through the suction plate from side walls, the pressure in the suction boxes is variously changed, and $C_P, C_{P_{SB}}^+, C_{P_{SB}}^-$ and the lift coefficient of the model are measured. Needless to say, the value of the lift coefficient is changed by the value of $C_{P_{SB}}^+, C_{P_{SB}}^-$. Next, $\Delta\alpha_S^*$ of various cases is found with these measured values, and it is plotted on a $C_L - \Delta\alpha_S^*$ surface with C_L at that time as Figure 14. The straight line which goes through these points shows the value of the lift coefficient in the case when the point, which crosses the C_L axis, becomes $\Delta\alpha_S^* = 0$. /12

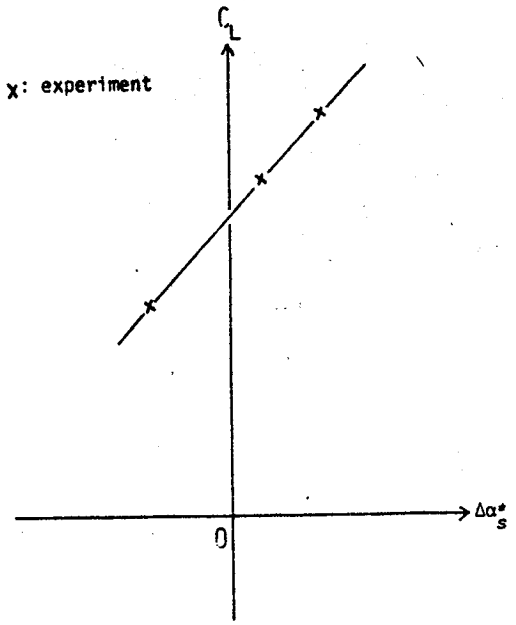

Figure 14. $\Delta\alpha_s^*-C_L$ surface.

4. Applications of this method for evaluating the influence of suction from the side walls in the two dimensional wind tunnel of the National Aerospace Technical Laboratory

The test section of the two dimensional wind tunnel has a width 300 mm, height 1000 mm, and the upper and lower walls consist of walls with multiple slots. NACA64A410 is used for the airfoil model matrix and airfoil chord length is 250 mm. Suction of fluid in the test section from side walls is achieved through a permeable disk of sintered metal. The effective diameter of the suction box side of this disc is 460 mm, so it was considered that the effective configuration of the suction plate was a 460 mm diameter disc. In the beginning, a disc shape was used for this suction plate, but later it was modified to a half disc shape in which the sealed bottom half was used. In this report only the experimental result of uniform Mach number 0.50, total pressure 4.0 kg/cm^2, and stagnation point temperature of about 20°C was used. Please refer to [4] for the details of the experiment.

Until the last section we stated a method of evaluating quantitatively the influence on the effective angle of attack of an airfoil. If the pressure distribution on the suction plates of the test section and pressure in suction box are known, suction of fluid in test section through the suction plate influences effective angle of attack of the airfoil model. However, static pressure pores, etc. to measure pressure distribution at the plate are not installed in the suction plate in this experiment. So, we decided to assume the pressure distribution across this suction plate from the pressure distribution of the central cross section of the airfoil model matrix. First of all, since airfoil model pressure distribution at the central cross section of airfoil model matrix was accurately found, static distribution over the entire flow area in the case when the pressure distribution occurs was found by using the thin airfoil approximation. The influence of upper and lower walls toward pressure distribution across the suction plate in the test section of the two dimensional wind tunnel of this laboratory becomes, at the highest, of the order 10^{-2} of the coefficient of static pressure. On the other hand, the influence which the airfoil model exerts on pressure distribution across the suction plate is 1 order higher than that. Therefore, in the case when the static pressure distribution over the flow area was found, the influence of upper and lower walls was ignored. Figure 15 shows the example of pressure distribution on a suction plate which was found as above.

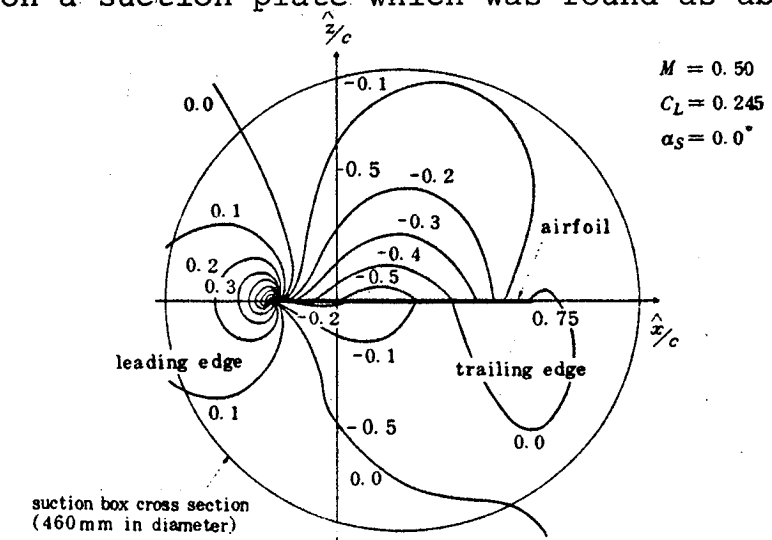

Figure 15. Lines of constant pressure on suction plate.

Since the thin airfoil approximation is used, this pressure distribution is not accurate near the leading edge of airfoil model; pressure distribution around this area is not so closely /13 related to the influence of suction front the side walls of the test section on the effective angle of attack of the airfoil model. This is because the velocity component perpendicular to the side walls around this area does not influence the effective angle of attack of the airfoil model. Figure 16 shows how strongly the velocity component which is perpendicular to sidewalls influences the upwash at the 1/4 airfoil chord length point of airfoil model, $\varphi_z^*(0, \pm 0)$ which is directly related to upwash and downwash by equation (49).

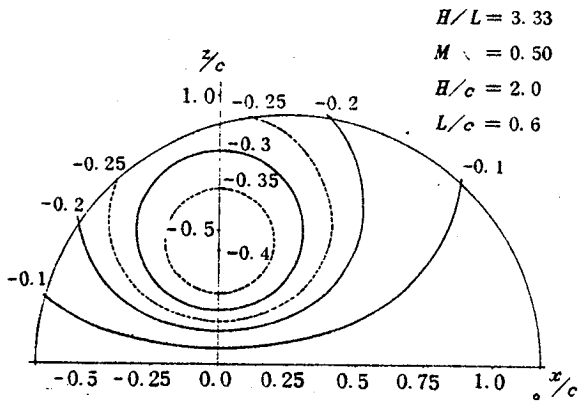

Figure 16. Weight function of v_n .

Symbols show distinction of upwash and downwash, and the absolute value shows the strength of the influence. This figure was found by using equations (28)' and (32). As understood from the figure, the velocity component perpendicular to the side walls very near the x axis does not influence the effective angle of attack of the airfoil model so much, compared to the kind of velocity component which is at a point some distance away from x axis. However, if λ is large -- namely, in the case when the space between side walls is very small compared to the height of the test section -- it is understood from Figure 17 that the velocity component perpendicular to the side walls near the x axis also sufficiently influences the effective

angle of attack of the airfoil model. In this case since the influence of the complex three dimensional boundary layer which occurs at the region where the side walls and the airfoil model matrix are connected influences the effective angle of attack of airfoil model as it is, applying the suction effect evaluation method of the suction effect found in the last section for this kind of influence evaluation must be avoided. The test section which is handled in this section is equivalent to the case of Figure 16.

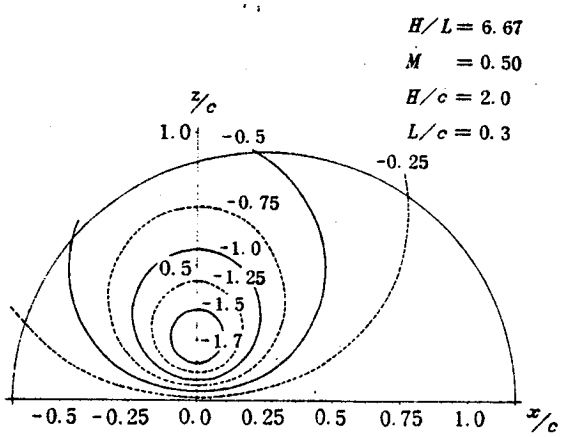

Figure 17. Weight function of v_n .

As mentioned before, the suction plate was completely orbicular for the two dimensional wind tunnel at the National Aerospace Laboratory. When this kind of suction plate is installed in the test section, flow occurs across this suction plate from pressure surface side of airfoil model matrix to suction surface side. Because of that, the absolute value of the lift coefficient becomes much smaller compared to the case in which side walls are made with solid walls and also in which the velocity component perpendicular to this kind of wall is only rarely derived. This aspect is shown in Figure 18.

Figure 19 shows upwash distribution on airfoil surface which is derived by suction from side walls.

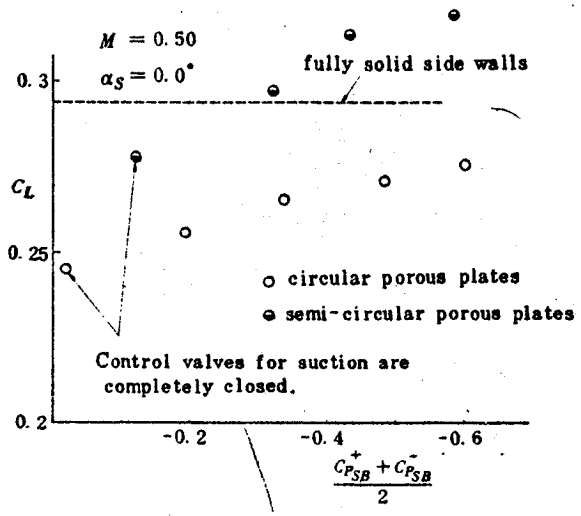

Figure 18. Effect of suction from an orbicular shaped suction plate.

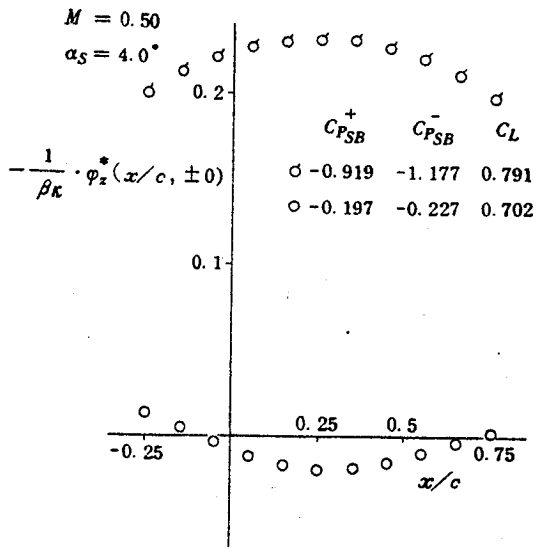

Figure 19. Upwash distribution on airfoil surface which was derived by suction from side walls. /14

Although it seems that the upwash angle is changed very much on the airfoil surface, the value of k is extremely small. In fact it is said that there is almost no change in upwash angle on the airfoil surface. Figure 20 shows the configurational change of the airfoil model in the case when the actual airfoil model received upwash angle distribution in the case of $\alpha_S = 4.0°$

in Figure 19 by the suction from side walls, by using a k value of 0.0476 which was determined logically later.

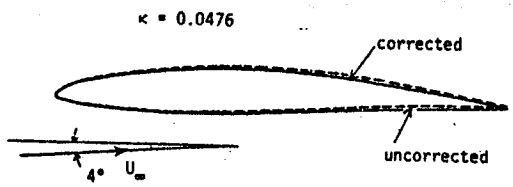

Figure 20. Airfoil model after revision (NACA 64A410).

As understood from the figure, the camber configuration of the airfoil model almost did not change. This type of airfoil model configuration rarely changes in the experimental results handled in this report; the influence was received as a change of the effective angle of attack. We are going to discuss the influence exerted on the lift coefficient from side walls by suing only $\Delta\alpha_S^*$ which as a proportional relationship with the increment $\Delta\alpha_S$ of the effective angle of attack of the airfoil model with suction from the side walls.

Figure 21 shows a combination of $\Delta\alpha_S^*$ and C_L which are toward various pressures in suction box plotted on an $\Delta\alpha_S^*$-C_L surface.

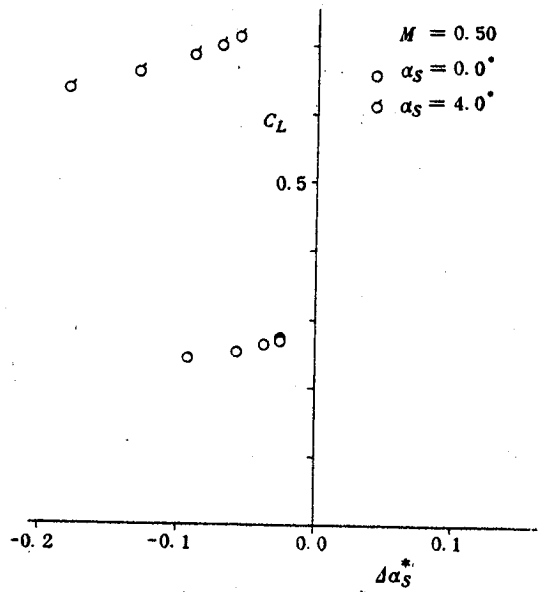

Figure 21 C_L vs. $\Delta\alpha_S^*$. /15

As is understood from this figure, even if the pressure in the suction box is changed variously, (in this case as the pressure of suction box is lowered, marks ○ and ▽ move to their right), $\Delta\alpha_s^*$ which is derived from the suction does not become 0. Namely, flow x occurs in this orbicular suction plate from the pressure surface of airfoil model through the suction plate toward suction surface. And even if the pressure of the suction box is lowered extremely, it shows that the influence toward $\Delta\alpha_s^*$ barely disappears. If the pressure in the suction box is lowered in order to weaken the flow of fluid in the suction box to the test section through the suction plate toward the pressure distribution on the suction plate on the suction plate side of the airfoil model, a flow toward the suction box occurs from the larger test section through the suction plate on the pressure surface side of the airfoil model. Therefore, in order to avoid this bad circulation, the suction plate was remodeled to one in which the lower half of this disc shaped suction plate was sealed up. Because of that, even in the case when the valve that controls the amount of suction is completely closed, as shown in Figure 18 the lift coefficient, at the time when the suction plate with this airtight lower half was installed, became very close to the case in which the sidewalls are completely solid walls. Since this half orbicular suction plate is the original orbicular suction plate with the lower section sealed up it has completely the same pressure loss coefficient as the orbicular suction plate. Namely, the undetermined constant k, which appeared in the last section, is the same for the orbicular suction plate and the half orbicular suction plate. Figure to Figure 26 show the combination of $\Delta\alpha_s^*$ and C_L obtained by suction effect experiments using the above two kinds of suction plates, plotted on a $\Delta\alpha_s^*$-C_L surface. From these figures in the case when there is no influence of suction from the side walls on the effective angle of attack of the airfoil model, C_L is found when $\Delta\alpha_s^*$ is 0, and the one which is plotted on C_L-α_s surface is Figure 27.

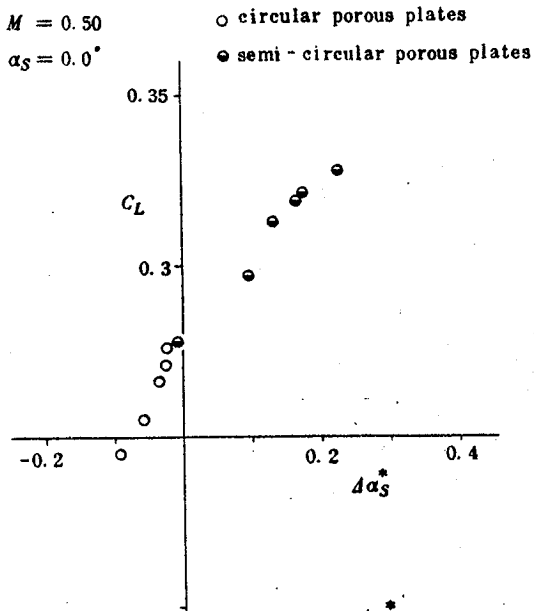

Figure 22. C_L vs. $\Delta\alpha_S^*$.

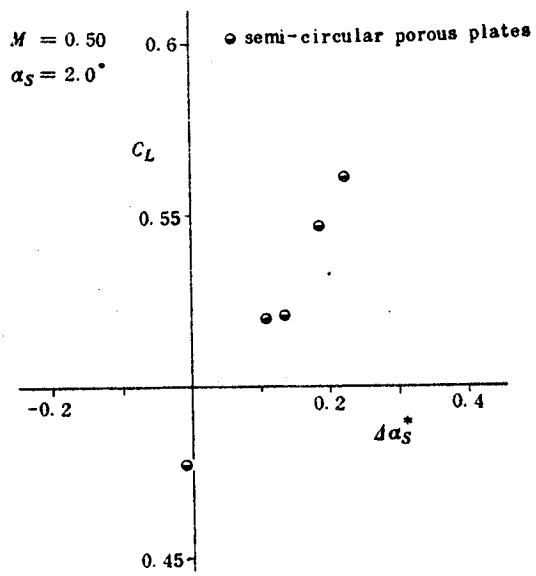

Figure 23. C_L vs. $\Delta\alpha_S^*$.

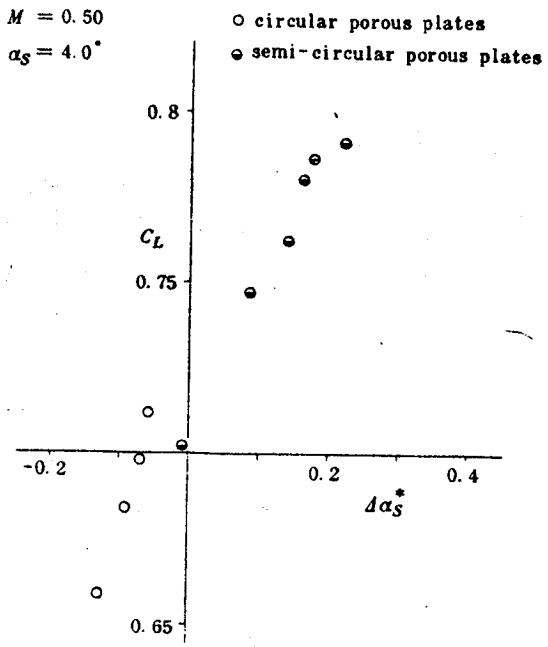

Figure 24. C_L vs. $\Delta\alpha_S^*$.

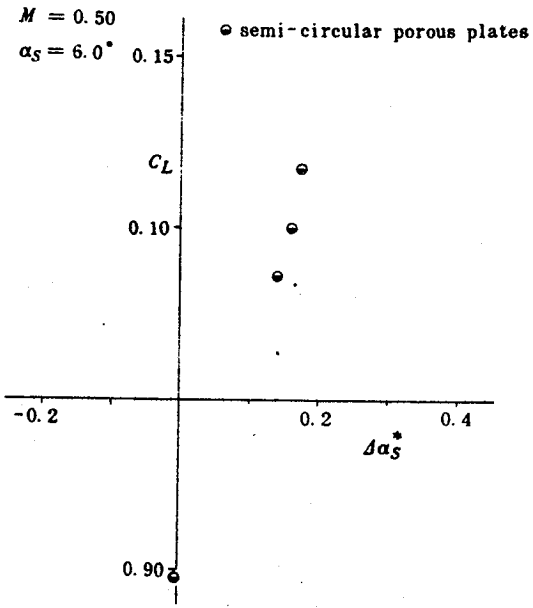

Figure 25. C_L vs. $\Delta\alpha_S^*$.

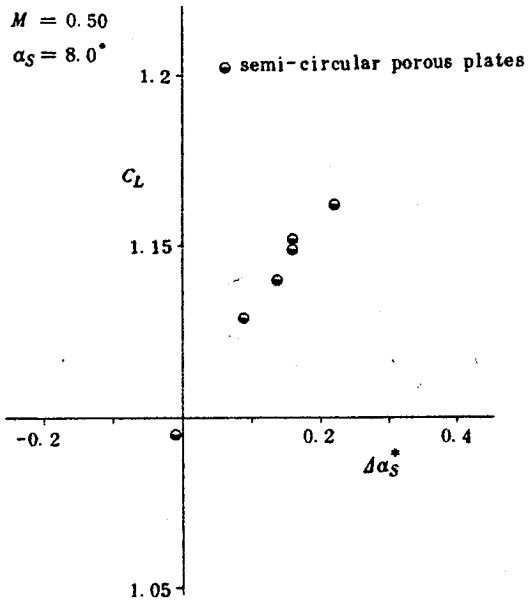

Figure 26. C_L vs. $\Delta\alpha_S^*$.

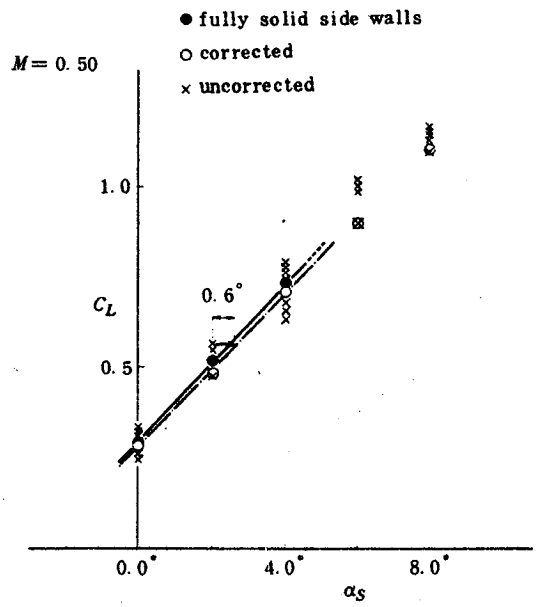

Figure 27. Lift coefficient curve. /16

In this figure the lift coefficient which was obtained when the pressure in suction box was variously changed is shown as is, by mark x. Also, at the same time the relationship between

the setup angle of attack when the side walls are completely solid walls and the lift coefficient is shown. It is considered that the lift coefficient for which the suction effect was eliminated from the side walls which was found from the various lift coefficients, has been corrected, although this is somewhat smaller than the lift coefficient for which the side walls are completely solid. It is also considered that those differences which still remain occurred because of the insufficient accuracy of the static distribution on the suction plate, approximation differences in the velocity components perpendicular to the suction plate, and differences which occurred because ignorance of boundary layer developed on side walls. A more accurate approximation and experience will be necessary in the future. The curve of lift coefficients obtained by the correction of suction efficiency from side walls is shown as a broken line in Figure 27. It is understood from the figure that at a set angle of attack of 2 degrees, the effective angle of attack of the airfoil model which creates a lift coefficient at the time when the pressure in suction box is lowered maximally is 2.6 degrees. If the k value is determined for $\Delta\alpha_s$ to become 0.6 degrees, the value becomes 0.0476. If the k value is determined and if this k value is substituted into other experiments, the increment $\Delta\alpha_s$ of the effective angle of attack is found as a numerical value. Figure 28 is a plot of the relationship between effective angle of attack $\tilde{\alpha}_s$ of airfoil model after revision obtained as above, and C_L . As long as the setting of the angle of attack does not become more than 8 degrees, it is said that they are almost on one straight line. /17

In the case when uniform Mach number is high and a supersonic area occurs on the airfoil surface, as the basic equation of the flow area is not described by a linear type Laplace equation, this method cannot be used. However, as long as the supersonic domain on airfoil surface does not become very large, it is recognized from experience that the usual method of subsonic wall interference correction can be practically applied. Therefore,

the writers think that it is worthwhile to apply this method to the case in which shock waves occur on the airfoil surface. Needless to say, pressure distribution on the suction plates must be found by using analysis of non-linear flow areas from the static distribution on airfoil surface.

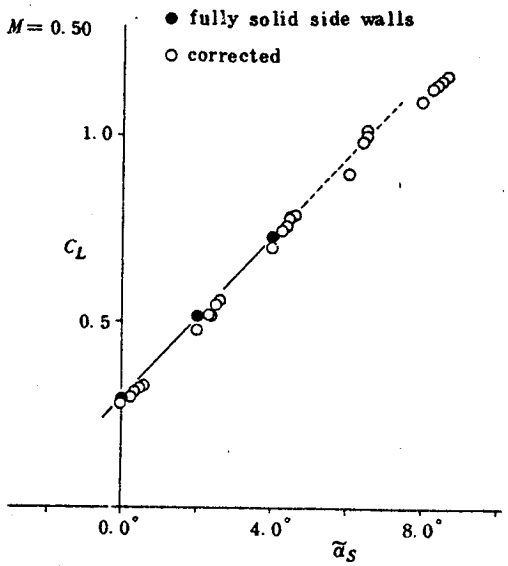

Figure 28. Plot of the effective angle of attack and C_L for k = 0.0476.

5. Conclusion

In the wind tunnel where performance testing of two dimensional airfoil model matrixes is done, the space between the side walls of the test section is made extremely narrow compared to the height. We handled the wall interference of this kind of test section by considering the existence of the side walls. As a result, it was understood that wall interference of this kind of wind tunnel test section is basically described by the summation form of wall interference in the case of two dimensional flow and the interference of side walls. Also, an equation in which the quantitative evaluation of side wall interference is possible if the distribution on a test surface which is set near the velocity component perpendicular to the side walls

is known. By using the evaluation equation, the influence on the effective angle of attack of airfoil model matrix in the case when fluid in test section was sucked through suction plate from side walls was studied, and a lift coefficient was determined for the case in which the influence on the effective angle of attack of the airfoil model matrix was considered. The curve of lift coefficients which was found as above became very close to the case of solid side walls.

Symbols

C_P : Pressure coefficient, equation (35)

$C_{P_{SB}}$: Pressure coefficient in suction box, equation (36)

$C^{+}_{P_{SB}}$: Pressure coefficient of the right side suction box in Figure 13

$C^{-}_{P_{SB}}$: Pressure coefficient of the left side suction box in Figure 13

c : Airfoil chord length (-250 mm)

g : Equation (18)

H : Wind tunnel half height converted by equation (4)

$\mathcal{H}$: An arbitrary function regarding (ξ, η, ζ)

h : Equation (19)

$J_B^{(n)}(x;\lambda)$: Equation (24)

$J_U^{(n)}(x;\lambda)$: Equation (30)

$J_V^{(n)}(x;\lambda)$: Equation (29)

K : Pressure loss coefficient, equation (33)

$K_0(x)$: Transformed Bessel function $K_n(x)$, n=0

$K_1(x)$: Transformed Bessel function $K_n(x)$, n=1

k : Equation (12)

L : Wind tunnel half width transformed by equation (4)

M : Uniform Mach number

P : Static pressure at each point of flow

P_{SB} : Internal pressure of suction box

P_∞ : Uniform static pressure

$S(\xi, \eta)$: Width distribution of airfoil

S_w : Figure 1 ($S_w = S_{wing} + S_{wake}$)

S_{wing} : Figure 1

S_{wake} : Figure 1

$S_2(\xi)$: Width distribution of two dimensional airfoil model

U_∞ : Uniform flow speed

(u, v, w) : (ϕ_x, ϕ_y, ϕ_z)

$u_{HC}^{a(n)}$: Equation (31)

$v_{LC}^{a(n)}$: Equation (26)

$v_{LS}^{a(n)}$: Equation (32)

$v_{LS}^{a(n)+}$: Equation (44)

$v_{LS}^{a(n)-}$: Equation (45)

v_n : Speed component perpendicular to Σ_L, Σ_L surface

$w_{HC}^{a(n)}$: Equation (27)

(x, y, z) : $(\hat{x}, \hat{y}, \hat{z})$ transformed by equation (4), Figure 2

$\hat{x}$: Distance from 1/4 airfoil chord length point of airfoil model

x_L : down stream along with tunnel axis

x_T : x coordinates of leading edge

coordinates of trailing edge

$\hat{y}$: Distance from $\hat{x}$ axis to airfoil model matrix span direction, (Refer to Figure 2 for a symbol)

$\hat{z}$: Perpendicular and upward distance from $\hat{x}$ axis

$\tilde{\alpha}_S$: Angle of attack of airfoil model in which the airfoil model matrix at the time when the space between side walls become infinite at test section incurs the same lift coefficient as wind tunnel test.

α_S : Angle of attack of airfoil model of wind tunnel test

β : Prandtl - Clauert number, equation (5)

$\Delta\alpha_S$: Equation (50)

$\Delta\alpha_S^*$: Equation (51)

Φ : Velocity potential in wind tunnel

$\tilde{\Phi}$: Velocity potential in free flow

ϕ : Minute disturbance potential in wind tunnel

$\tilde{\phi}$: Minute disturbance potential in free flow

φ : Wind tunnel wall interference potential equation (21)

φ_z^* : Equation (47)

Ψ : Equation (11)

$\tilde{\Psi}$: Equation (6)

ρ_∞ : Uniform flow density

λ : H/L

κ : Equation (40)

$$\mathrm{sgn}(x): = \begin{cases} 1 & \text{for } x > 0 \\ -1 & \text{for } x < 0 \end{cases}$$

$$\mathbb{1}(x): = \begin{cases} 1 & \text{for } x > 0 \\ 0 & \text{for } x < 0 \end{cases}$$

REFERENCES

1. Bernard-Guelle, R., and Chevallier, Jean Pierre. Lateral Boundary Layer Effects on Two Dimensional Tests, Paper presented at 48th Annual Meeting of Supersonic Tunnel Association, Toulouse, Sept. 14-15, 1977.

2. Ohman, L.H.; The NAE High Reynolds Number 15 in.x60 in. Two-Dimensional Test Facility, Part I. General Information, NAE Report, LTR-HA-4, 1970.

3. Vaucheret, X., Bazin, M. and Armand, C.; Comparison D'essais Transsoniques Bl-et Tridimensionnels Effectues dans Diverses Grandes Souffleries, ONERA, T.P. n° 1975 - 61, 1975.

4. Seizo Sakakibara, and others, Preliminary test of boundary layer suction equation for two dimensional wind tunnel at National Aerospace Technical Laboratory, collected reports of the Japan Aerospace Academy 12th yearly lecture meeting, PP 136-137, 1981.

5. Sawada, H.; Wind Tunnel Wall Interference in a Test Section with Ventilated Walls, ICAS-80-23. 5, 1980.

6. Hideo Sawada, and others; Experiment about two dimensional lift interference of perpendicular pores in porous wall, NAL TR-563, 1979.